communications biology

Article

https://doi.org/10.1038/s42003-024-06966-0

First evolutionary insights into the human otolithic system

Christopher M. Smith [1,2] ✉, Romain David [3], Sergio Almécija [1,2,4], Jeffrey T. Laitman[2,5,6] & Ashley S. Hammond [1,2]

The human otolithic system (utricle and saccule), housed within the bony vestibule of the inner ear, establishes our sense of balance in conjunction with the semicircular canals. Yet, while the morphological evolution of the semicircular canals is actively explored, comparative morphological analyses of the otolithic system are lacking. This is regrettable because functional links with head orientation suggest the otolithic system could be used to track postural change throughout human evolution and across primates more broadly. In this context, we present the first analysis of the evolution of the human otolithic system within an anthropoid primate setting. Using the vestibule as a morphological proxy for the utricle and saccule, we compare humans to 13 other extant anthropoid species, and use phylogenetically-informed methods to find correlations with body size, endocranial flexion, and head-neck posture. Our results, obtained through micro-CT of 136 inner ears, reveal two major evolutionary transitions in hominoids, leading to distinctive vestibular morphology in humans, characterized by otolithic morphology resembling squirrel monkeys (possibly due to reversal), with a pronounced supraovalic fossa. Finally, we find a positional signal embedded in the anthropoid bony vestibule, providing the foundation to further explore the evolution of human head-neck posture using inner ear morphology.

The vestibular system is essential to human balance and motion. It is present in all vertebrates, and is fundamental to gaze stabilization, motor coordination, navigation, and spatial self-awareness[1]. Sensory organs of the vestibular system, collectively referred to as the "peripheral vestibular system," are comprised of fluid-filled soft-tissue structures forming the upper part of the so-called membranous labyrinth, itself housed within the bony labyrinth, a "shell" inside the petrous bone. In humans, the peripheral vestibular system comprises five paired sensory organs each mirroring the other across the mid-sagittal plane of the head. These include three semicircular ducts, which are enclosed by semicircular canals (SCCs), detecting head angular velocity, and two otolithic organs, the utricle and saccule, which are housed within the bony "entryway" of the labyrinth (hence *vestibule*) and detect head linear acceleration, vibration, and tilt relative to gravity[2] (Fig. 1).

Primates exhibit considerable morphological variation in their peripheral vestibular system[3–6], as well as exceptionally diverse positional behaviors[7,8], the evolution of these two components being somehow intertwined. As such, peripheral vestibular system morphology needs to be attuned for effective detection of behaviorally-induced head motion[9–13], while positional behaviors require adequate gaze stabilization and motor coordination, both depending on accurate head motion detection[14]. In this context, morphological differences in specific regions of the peripheral vestibular system (e.g., semicircular canal radius of curvature, semicircular canal orientation) have been studied to assess evolutionary shifts in the locomotor repertoire of primates[15–20], as well as to understand mammalian positional behavior more broadly[21–24].

While there is a growing interest in addressing aspects of primate peripheral vestibular system morphology, previous research has focused almost entirely on the SCCs. Arguably, the morphology of the otolithic organs—an evolutionarily ancient part of the peripheral vestibular system—remains largely unexplored in primates despite having a central role in vestibular functions. This is likely due to the fact that: (1) following the emergence of micro-CT scanning, anatomical research on the peripheral vestibular system shifted to focus on the bony labyrinth; and (2) it is difficult to identify the morphology of the utricle and saccule on the vestibule. This contrasts with the simpler morphological relationship existing between semicircular ducts and canals, and likely explains why

[1]Division of Anthropology, American Museum of Natural History, New York, NY, USA. [2]New York Consortium in Evolutionary Primatology, New York, NY, USA. [3]Centre for Human Evolution Research, Natural History Museum, London, UK. [4]Institut Català de Paleontologia Miquel Crusafont (ICP-CERCA), Universitat Autònoma de Barcelona, Barcelona, Spain. [5]Center for Anatomy and Functional Morphology, Icahn School of Medicine at Mount Sinai, New York, NY, USA. [6]Department of Otolaryngology, Icahn School of Medicine at Mount Sinai, New York, NY, USA. ✉e-mail: csmith2@amnh.org

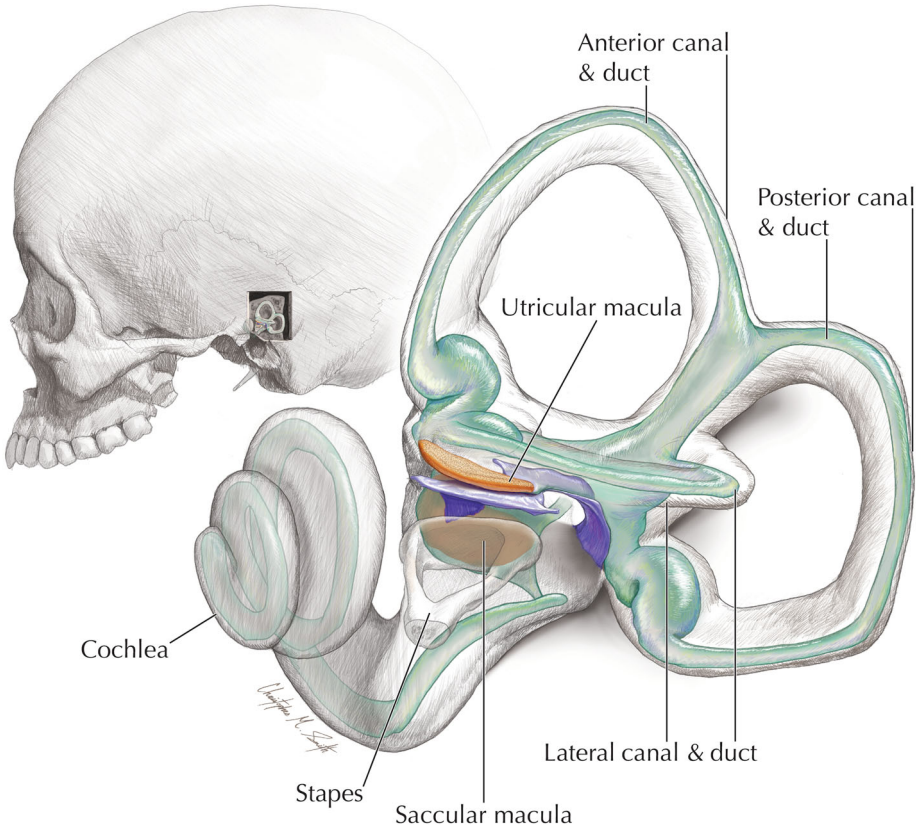

Fig. 1 | Human inner ear anatomy. Left lateral view of a human cranium shown on the top left with a cut bony window showing the inner ear within. The bottom right image shows the left inner ear enlarged. Membranous labyrinth shown in green; otolithic maculae shown in orange; the membrana limitans is in purple. Illustration by CMS. Modified from ref. 59.

otolithic organs are much less studied. Still, from the early twentieth century onward, research on the utricle and saccule occurred within a human clinical context[25–31], and were not focused on addressing evolutionary questions. As a result, information on how otolithic organs changed over time remains elusive, prohibiting a fuller understanding of primate evolution and, more specifically, of the evolution of human vestibular function and posture.

In theory, the morphology of the utricle and saccule, particularly of their hair cell covered sensory maculae, should provide evidence for changes in head orientation relative to both the neck and gravity axes (i.e., head and neck posture). The reason for this is that both the geometry and the orientation of their maculae directly affect the function of the otolithic organs, which is to detect head linear acceleration and tilt relative to gravity[32]. More specifically, two gross morphological variables are known to influence otolithic organ function. They are: (1) the orientation of the maculae relative to the gravity vector[26,33,34]; and (2) the surface area of the maculae, with a larger surface area providing increased sensitivity[32]. Consequently, head and neck posture may share a direct relationship with the shape and size of the otolithic sensory maculae, relationships that potentially extend to the vestibule, whose morphology relates to that of the otolithic organs [35]. In this context, looking at vestibule morphology should allow us to retrace the evolution of the otolithic organs in anthropoids (the monkey, ape, and human clade), and to pinpoint morphological changes happening concomitantly with positional behavior shifts, such as the advent of orthogrady and the later emergence of obligate bipedalism in hominins (i.e., humans and our closest extinct relatives).

In this study, we examine the vestibular morphology of anthropoids, using 3D geometric morphometrics and phylogenetically informed methods, to better understand the evolution of the otolithic organs and uncover relationships they share with head and neck posture. To do so, we first describe the shape and size of the vestibule, then assess how both relate to (1) anthropoid phylogeny, (2) body mass, (3) endocranial flexion, and (4) head and neck orientation metrics.

Results

Gross vestibule morphology

Anthropoid primates exhibit considerable variation in the shape of their vestibule (Fig. 2), most likely reflecting differences in position, orientation, and relative size of both the utricle and saccule. Among anthropoids, hominoids (i.e., apes and humans) show the highest morphological diversity, with African great apes (i.e., chimpanzees and gorillas) possessing a spherical recess (housing the saccule) that is flattened and inferiorly displaced (*Pan troglodytes*, *Gorilla gorilla*; Fig. 2), whereas it is enlarged and more rounded in humans, orangutans and siamangs (*Homo sapiens*, *Pongo pygmaeus*, *Symphalangus syndactylus*; Fig. 2). Additional features distinguish hominid (i.e., great ape and human) taxa from other anthropoids, including a relatively enlarged utricular region in all hominids (Fig. 2), more pronounced supraovalic fossa in humans (Fig. 3), located between the lateral ampulla and the oval window (also called the fenestra ovalis), and a superiorly displaced utricular region of the vestibule in chimpanzees (Figs. 2B and 4).

Vestibule shape

The first axis (PC1; Fig. 4) of a principal components analysis (PCA) of vestibule shape, analyzed via geometric morphometrics, separates hylobatids (i.e., gibbons—*Hylobates lar* in this case—and siamangs) from hominids, with cercopithecids (i.e., Afroeurasian monkeys) placed more intermediate and a more dispersed distribution in platyrrhines (i.e., Panamerican monkeys). Within hominids, we see a slight gradient in species' shape means, with chimpanzees being the closest to hylobatids and humans plotting the farthest away. This axis reflects major differences in the position and orientation of the utricular region, in saccule shape, and in the position of the aqueductal junction (i.e., the inferiormost point where the vestibular aqueduct meets the posterior semicircular canal). Hylobatids (positive values) are characterized by an anterolateral-posteromedially compressed saccule, a superiorly displaced aqueductal junction, and a utricular region that is anteriorly displaced and rotated posteromedially. This is in contrast

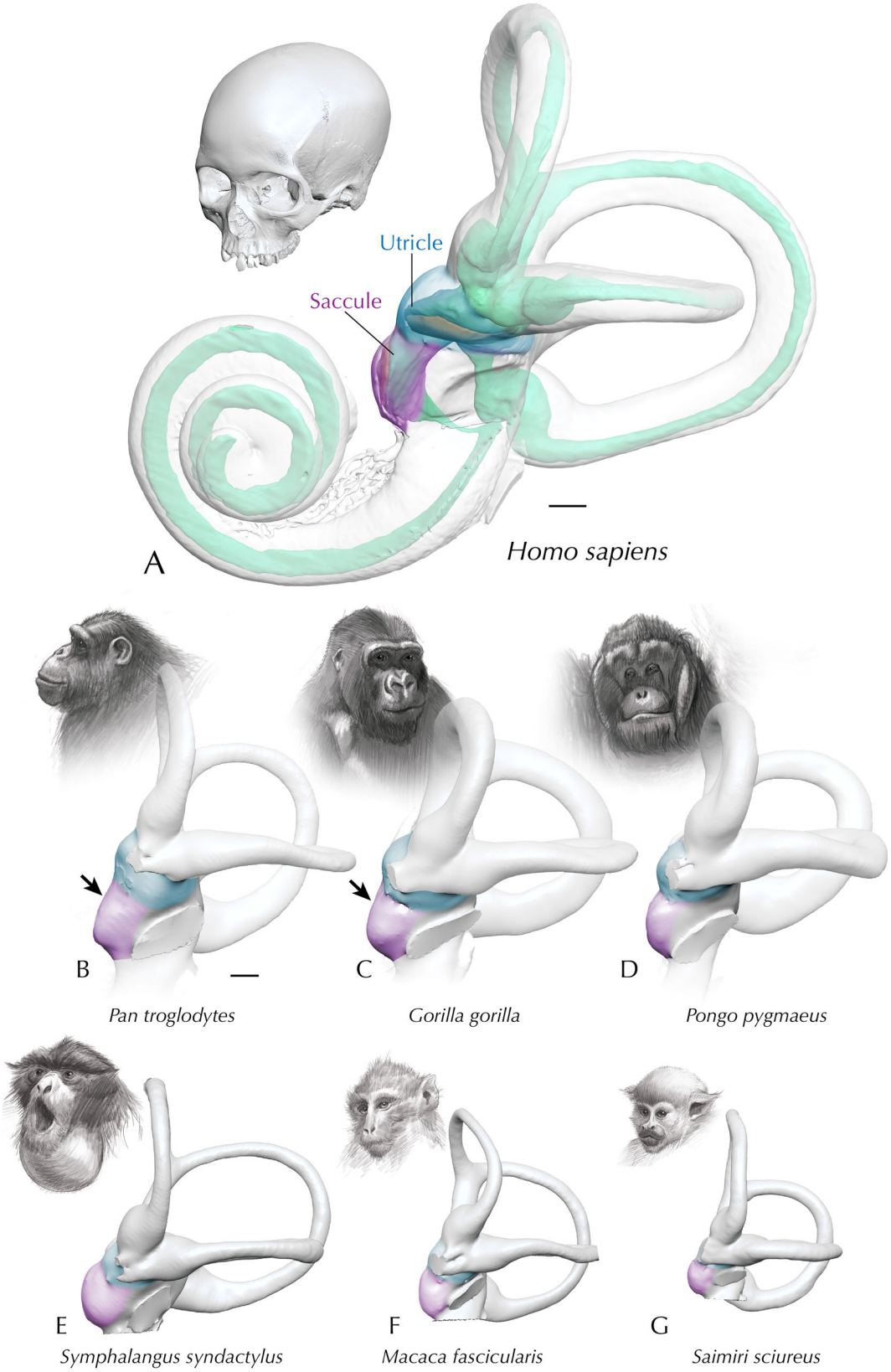

Fig. 2 | Anthropoid vestibular morphology. A Anterolateral view of the left inner ear in humans. Membranous labyrinth (green), including otolith organ maculae (orange), shown beneath a transparent bony labyrinth. Cranium shows head orientation. The utricular (blue) and saccular (purple) regions of the vestibule are highlighted among great apes (**B**–**D**) and three species of other anthropoids (**E**–**G**). Arrows indicate the flattened, inferiorly displaced spherical recess (that houses the saccule) in African great apes. 3D models derived from μCT scans. Scale bars = 1 mm. Primate portrait illustrations by CMS.

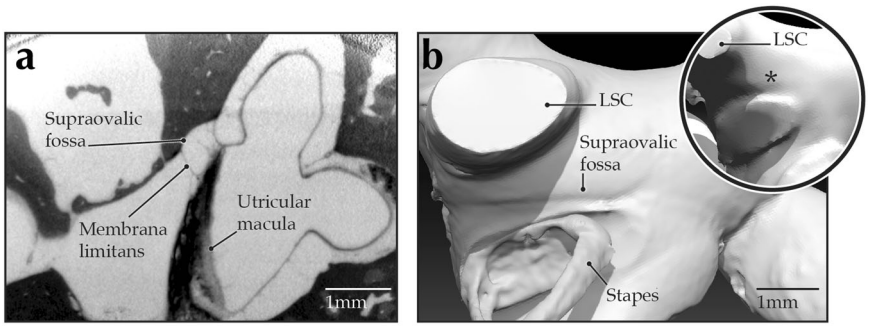

Fig. 3 | The distinctive human supraovalic fossa. **a** Micro-CT (μCT) image showing the location of the fossa in the inner ear; **b** 3D digital model of the bony labyrinth depicting the supraovalic fossa (derived from the μCT stack in **a**). LSC lateral semicircular canal. Inset shows the supraovalic fossa (asterisk) in *Pan troglodytes*. Modified from ref. 59. Scale bars = 1 mm.

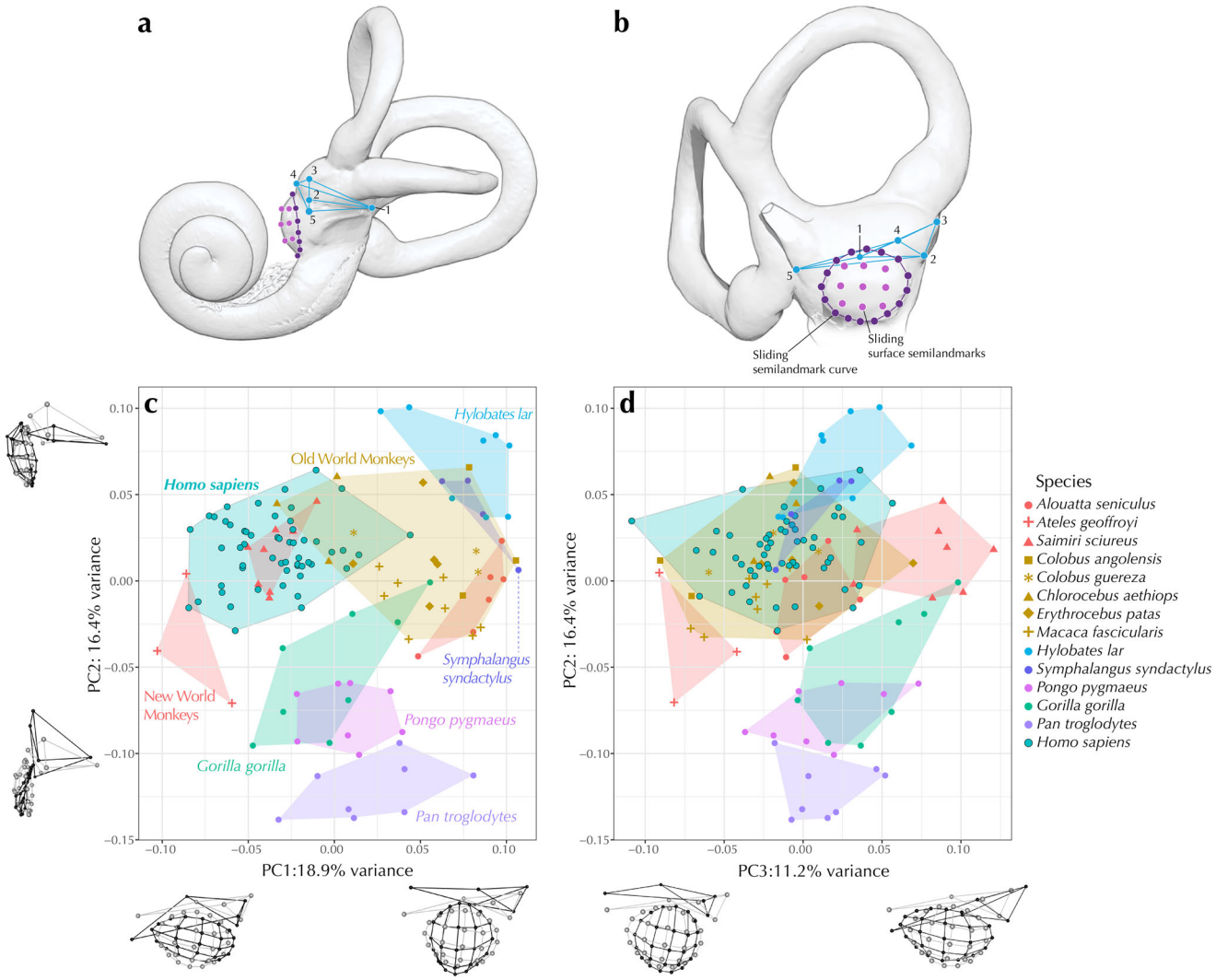

Fig. 4 | Landmarks and bivariate PCA plots of vestibule shape in anthropoid species. The human bony labyrinth is shown in anterolateral view (**a**) and anteromedial view (**b**), with blue landmarks indicating the bony structure of the utricle. Purple landmarks indicate the bony structure of the saccule (also known as the spherical recess). **c** PC1 against PC2. **d** PC2 against PC3. Gray wireframes indicate the average configuration of landmarks describing vestibule shape. Black wireframes indicate extreme landmark configurations along each axis, exaggerated by a factor of 2. Wireframes are shown from an antero-medial view for PC1 and PC3, and from an antero-lateral view for PC2, to best visualize the greatest shape differences.

with the condition observed in hominids and particularly in humans (negative values), which includes a supero-inferiorly compressed saccule, an inferiorly displaced aqueductal junction, and a utricular region, which is located directly superior to the saccule and rotated anterolaterally.

The second axis (PC2, Fig. 4) separates hylobatids from great apes, with monkeys and humans being intermediate. Within hominids, we again see a gradient in species' means, but this time, humans plot closest to hylobatids, and chimpanzees plot the farthest away. This axis relates to the relative size, positioning, and orientation of the utricular and saccular regions of the vestibule. Hylobatids (positive values), and humans to a lesser extent, show a supero-inferiorly compressed utricular region aligned with the top of the spherical recess, which is expanded medio-laterally, and an acute angulation

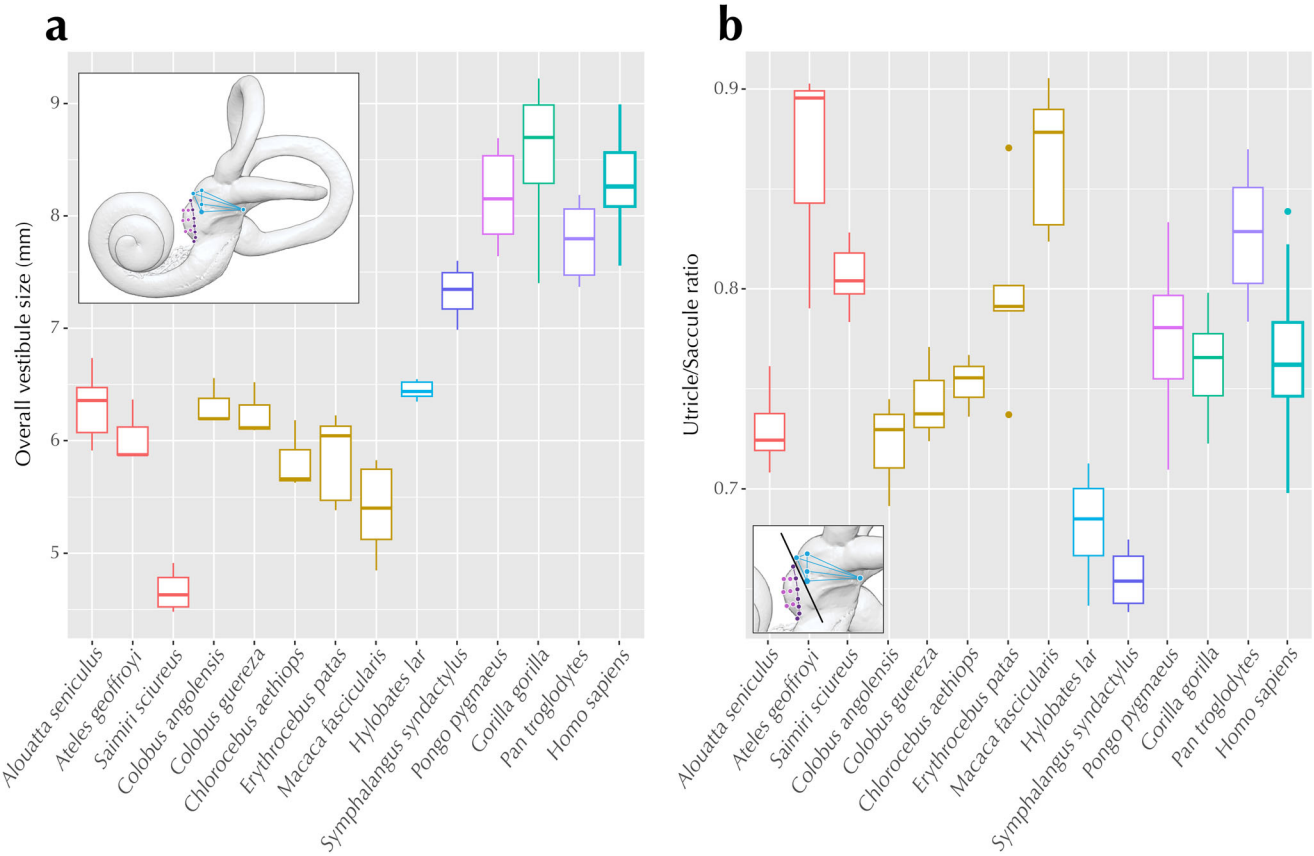

Fig. 5 | Size variation in the anthropoid vestibule. Box plots of **a** vestibule centroid size and **b** US ratio. The lower and upper bounds of the boxes, respectively, represent the first and third quartiles, the thick bar represents the median value, and the top and bottom bounds of the whiskers, respectively, represent maximum and minimum values. Dots represent outliers following the interquartile range criterion.

Table 1 | Phylogenetic signal in vestibule size and shape

Explanatory variable	Pagel's λ	logL	*p* value	Bloomberg's K/K_{mult}	*p* value
Vestibule centroid size	0.999	−16.16	**0.001**	1.56	0.001*
US ratio	<0.0001	19.70	1	0.64	0.055
Overall vestibule shape	0.249	445.92	0.516	0.51	0.004*
MA	<0.0001	−43.39	1	0.24	0.944

Asterisks indicate significant *p* values.
logL log likelihood, *MA* estimated angle between utricular and saccular maculae, *US ratio* ratio between centroid sizes of utricular and saccular regions.

between the inferred utricular and saccular maculae. On the contrary, great apes (negative values) are characterized by a supero-inferior expansion of the utricular region, displaced superiorly relative to the spherical recess, itself compressed medio-laterally, and an obtuse angulation between the inferred utricular and saccular maculae.

The third axis (PC3, Fig. 4) shows considerable overlap in morphospace, and only separates squirrel monkeys (*Saimiri sciureus*) from spider monkeys (*Ateles geoffroyi*), all other species being intermediate between these two. As with the first axis, morphological variation along this axis is primarily driven by the position and orientation of the utricular region, saccule shape, and the position of the aqueductal junction. Squirrel monkeys (positive values) present an anterolateral-posteromedially elongated saccule, an inferiorly displaced aqueductal junction, and an anteriorly displaced utricular region that is rotated posteromedially. This contrasts with spider monkeys, characterized by an anterolateral-posteromedially compressed saccule and an aqueductal junction aligned with the utricular region, itself located just above the saccule and rotated anterolaterally.

Vestibule size

Among anthropoids, hominids possess the largest vestibules, with hylobatids being intermediate between them and other anthropoids (Fig. 5a). The cynomolgus monkey (*Macaca fascicularis*) and the spider monkey are characterized by the highest ratio between the sizes of the utricular and saccular regions (US ratio hereafter), while gibbons and siamangs show the exact opposite, a direct consequence of their enlarged spherical recess (Fig. 5b). Among hominids, chimpanzees possess the smallest vestibules and the highest US ratio, while gorillas (*Gorilla gorilla*) have the largest vestibules and a US ratio similar to that of humans and orangutans.

Phylogenetic signal of the vestibule

The vestibule centroid size of anthropoids contains a strong, significant phylogenetic signal ($\lambda = 0.99$, $p = 0.001$; $K = 1.57$, $p = 0.001$; Table 1), with closely related species being more similar than what would be expected under a Brownian motion model of evolution. Conversely, the phylogenetic signal of overall vestibule shape (i.e., Procrustes coordinates) is weaker, and only Blomberg's K value is significant ($\lambda = 0.25$, $p = 0.516$; $K_{mult} = 0.51$,

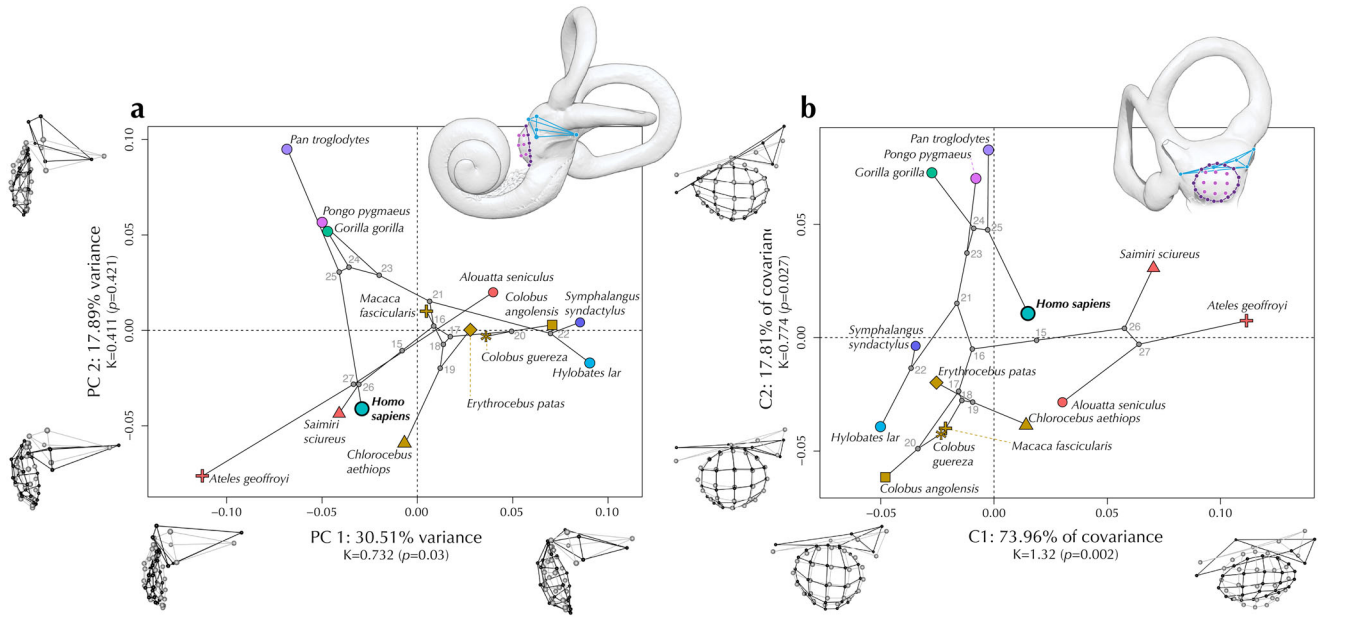

Fig. 6 | Evolution of the anthropoid otolithic system. Phylomorphospaces based on **a** a principal component analysis and **b** a phylogenetically-aligned component analysis of Procrustes shape coordinates of the vestibule. Both plots show the first and second components of the analyses, with the percentage of variance they explain and the phylogenetic signal they carry. Blue landmarks on the top insets indicate the bony structure of the utricle. Purple landmarks indicate the bony structure of the saccule (also known as the spherical recess). Wireframes depict landmark-based shape differences along each axis. Gray wireframes indicate the average configuration of landmarks describing vestibule shape. Black wireframes indicate extreme landmark configurations along each axis, exaggerated by a factor of 2. Wireframes are either shown from **a** an antero-lateral view or **b** an antero-medial view to best visualize the greatest shape differences. Numbers indicate ancestral state estimations for the following clades: 15-Anthropoidea, 16-Catarrhini, 17-Cercopithecidae, 18-Cercopithecinae, 19-Cercopithecina, 20-Colobinae, 21-Hominoidea, 22-Hylobatidae, 23-Hominindae, 24-Homininae, 25-Hominini, 26-Platyrrhini, 27-Atelidae.

$p = 0.004$), indicating closely related species being less similar than what would be expected under Brownian motion. No phylogenetic signal was found for either the US ratio ($\lambda = <0.0001$, $p = 1$; $K = 0.64$, $p = 0.55$; Table 1), nor for the estimated angle between the utricular and saccular maculae (MA hereafter; $\lambda < 0.0001$, $p = 1$ and $K = 0.24$, $p = 0.944$; Table 1).

Mapping anthropoid phylogeny onto the first and second axes of a between-group principal component analysis of vestibule shape, considering a strict Brownian motion model of evolution, we obtain a phylomorphospace where the ancestral state estimation for the nodes of hominoids and catarrhines fall close to the origin of the plot (PC1-2, Fig. 6a). Among extant species, the cynomolgus monkey and, to a lesser extent, humans and the common patas monkey (*Erythrocebus patas*) plot the closest to this ancestral state estimation. Divergent morphologies between sister taxa can be observed in this phylomorphospace, as exemplified by the spider monkey and the Colombian red howler monkey (*Alouatta seniculus*), or by humans and chimpanzees. In particular, the human/chimpanzee split spans the second axis, with chimpanzees exhibiting an exaggerated hominid morphology with a supero-inferior expansion of the utricular region and a spherical recess that is medio-laterally compressed and displaced inferiorly, while humans show a large spherical recess that is positioned at the same height as the utricular region, itself compressed superoinferiorly.

A phylogenetically-aligned component analysis (Fig. 6b) indicates that, among anthropoids, phylogenetic signal is mostly found in both the orientation of the utricular region and the shape of the saccule (C1), as well as in the positions of the utricular region (C2) and the aqueductal junction (C1–2). In this phylogenetically informative morphospace, we observe a clear separation of platyrrhines (C1, positive values) and hominids (C2, positive values) from hylobatids and cercopithecids (C1–2, negative values). In this analysis, humans fall the closest to the ancestral state estimation for the last common ancestor of anthropoids (this ancestral state reconstruction, however, should be treated as preliminary, given our small sample of platyrrhine species).

Allometric and positional signals in the vestibule

Among tested explanatory variables, phylogenetic generalized least square (pGLS) regressions indicate that body mass is the only variable that can explain a large and significant amount of variation in vestibule centroid size ($R^2 = 0.85$, $p = <0.001$) (Table 2; see Supplementary Table 1 for additional models). Together with centroid size, body mass also explains a significant amount of variation in the ratio between centroid sizes of utricular and saccular regions (US ratio, $R^2 = 0.39$, $p = 0.0110$) (Table 2; see Supplementary Table 2 for additional models), suggesting that these regions follow different allometric trajectories, with the saccule growing faster with body mass than the utricle. Centroid size also explains a portion of shape variance in PCs 1, 4, 5, and 7, while US ratio explains shape variance in PCs 1, 2, 5, 6, and 7 see Supplementary Table 3 for regression results between vestibule size and shape components.

In contrast to centroid size and the US ratio, none of the variables we tested could significantly explain variation in Procrustes shape coordinates of the vestibule, or in the estimated angle between utricular and saccular maculae (MA; Table 2 and Supplementary Tables 4 and 5). However, using phylogenetic ANOVA on principal components of vestibule shape instead of Procrustes coordinates, we found that body mass and US ratio significantly explain about 33%, and 42% of variation along PC1, respectively. PC1 itself explains 18.9% of vestibule shape variation. US ratio, CBA (a measure of endocranial flexion), and neck inclination significantly explain about 23%, 40%, and 20% of variation along PC2, respectively. PC2 itself explains 16.4% of vestibule shape variation (Table 3 and see Supplementary Fig. 1 for a summary of head and neck metrics). No tested variable could significantly explain vestibule shape variation along PCs 3 to 5 (Supplementary Table 5).

Discussion

This study provides the first insights into the evolution of the human otolithic system within the context of anthropoid primates. Our analyses show several morphological features of the bony vestibule that differentiate taxonomic groups. These include differences between: (1) hominoids and

Table 2 | Results of select of pGLS regressions of bony vestibule size (centroid size), US ratio, and MA with explanatory variables

Model	R^2	λ	Variable	Coefficient	p value
ln Centroid size~ln Body mass	0.852	1	Intercept	0.7625	$4.47\ 10^{-05}$*
			ln Body mass	0.1196	$1.53\ 10^{-06}$*
ln US ratio~ln Body mass + ln Centroid size	0.385	0	Intercept	0.3693	0.1584
			ln Body mass	0.1171	0.0110*
			ln Centroid size	−0.9199	0.0110*
MA~ln US ratio + Orbit inclination	0.386	0	Intercept	86.345	$2.50\ 10^{-09}$*
			ln US ratio	34.019	0.0532
			Orbit inclination	0.381	0.0532

Only models with lowest AICc are shown here. All tested models can be found in Supplementary Table 4. Asterisks indicate significant *p* values. *p* values are adjusted using the Benjamini and Hochberg (fdr) method for multiple comparisons.
MA estimated angle between utricular and saccular maculae, *US ratio* ratio between centroid sizes of utricular and saccular regions.

Table 3 | Phylogenetic type I ANOVAs of principal components of vestibule shape

	Sum Sq	F	p value
Response: PC1, Lambda: 0, Delta: 1.42, Kappa: 3, $R^2 = 0.66$			
ln Body mass	2.38E−08	12.4135	0.044*
ln Centroid	3.64E−09	1.8928	0.495
ln US ratio	3.06E−08	15.9103	0.044*
CBA	3.66E−10	0.1907	0.791
Orbit inclination	3.60E−12	0.0019	0.967
Neck inclination	6.25E−10	0.3254	0.791
Frankfurt inclination	2.67E−09	1.3922	0.495
Residuals	1.15E−08		
Response: PC2, Lambda: 1, Delta: 3, Kappa: 3, $R^2 = 0.84$			
ln Body mass	7.44E−15	5.0312	0.090
ln US ratio	2.78E−14	18.7844	0.009*
CBA	4.90E−14	33.1197	0.004*
Orbit inclination	1.52E−15	1.0279	0.413
Neck inclination	2.47E−14	16.6665	0.009*
Frankfurt inclination	9.33E−16	0.6306	0.453
Residuals	1.04E−14		

Branch length transformations for Pagel's λ were optimized between set bounds using maximum likelihood. Asterisks indicate significant *p* values. *p* values are adjusted using the Benjamini and Hochberg (fdr) method for multiple comparisons. Centroid size is included as an additional variable in models in which shape components carry an allometric signal with the overall size of the vestibule. Phylogenetic type I ANOVAs of principal components 3 to 5 can be found in Supplementary Table 4.
CBA a measure of endocranial flexion (see "Methods"), *US ratio* ratio between centroid sizes of utricular and saccular regions.

cercopithecids, (2) hylobatids and hominids, and (3) humans and the African apes. Among hominoids, there is considerable morphological diversity of the vestibule, which contrasts with a more conserved morphology in cercopithecids. This diversity includes differences in the positioning, orientation, and relative size of the otolithic system. For example, great apes have a more superiorly displaced utricle relative to the saccule and a more obtuse angulation between the two. Hylobatids, instead, possess an enlarged saccule compared to all other anthropoids sampled. Such differences in bony configuration are tied to the location of the maculae and, in turn, sensory hair cell orientation (assuming that anthropoids share human-like integration of hard and soft tissues of the vestibule[35]). Due to this functional link, disparity among vestibule morphology could reflect differences in positional behavior, as differential macular orientation would alter sensitivity to certain directions of movement. This may include the more specialized postural repertoires among apes, particularly orthograde positioning of the head and torso[8,36,37].

In an evolutionary context, there are two major transformations in the hominoid bony vestibule. First, after the split between hylobatids and hominids and, second, after the split between *Pan* and *Homo* (Fig. 6a). The divergence of hylobatids and hominids relates to the size of the bony structure of the saccule relative to that of the utricle (see Figs. 4c and 6a), where the former is enlarged in hylobatids and reduced in the great apes. This enlargement suggests a similarly enlarged membranous saccule and saccular macula, which are known to be linked with bony structures in humans[35]. The saccule is primarily a detector of vertical linear acceleration in primates[11], and therefore, a relative increase in macula size may relate to increased sensitivity towards a vertical movement of the head. Considering the substantial portion of suspensory behavior and ricochetal brachiation within the hylobatid locomotor repertoire[37,38], an enlarged saccule may be adaptive for increased vertical movement with a heightened risk of vertical "drop." Furthermore, evidence for retained auditory sensitivity in the primate saccule (e.g., as observed in ref. 39) suggests a potential acoustic role in the enlarged saccule in hylobatids, particularly in siamangs who exhibit exceptionally loud and complex vocalizations (for further discussion, see refs. 40,41). Thus, the role of the otolithic system in detecting vibrations may have additional roles in behavioral evolution that remain to be fully explored.

The enlargement of the saccule is also linked with both body size and vestibule size, indicating that the divergence of hylobatids and hominids from the hominoid ancestral node may have an allometric component. Indeed, this type of allometry related to body size has also been observed in catarrhine facial morphology (including orbit shape and position[42]). If we assume, however, that the hominoid last common ancestor possessed a more hylobatid-like body size[43], then another variable (e.g., specialized locomotor modes or loud vocalizations) may be driving the derived hylobatid morphology. The inclusion of fossil taxa into the above analyses would enable more accurate reconstructions of ancestral morphologies, revealing how the otolithic system evolved alongside transitions in hominoid positional behavior.

African great apes, on the other hand, exhibit flattened and inferiorly displaced bony structures of the saccule, with medial expansion present only in the inferior portion of the spherical recess. This morphology may cause displacement of the saccular maculae, given that the macula itself adheres to the recess wall, from which the saccular nerve exits (for detailed anatomical descriptions, see ref. 44). This feature is indicated to have evolved away from a generalized hominoid morphotype more similar to cercopithecids (Fig. 6). The cause of this morphology is unknown but given the spherical recess's proximity to the pathway of the superior vestibular nerve (comprising the utricular and anterior and lateral ampullary nerves), compression of the superior portion of the recess could result from inferior displacement or relative enlargement of these nerves.

The second major evolutionary transformation is in both the *Homo* and *Pan* lineages (see Fig. 6a). In particular, the otolithic system in *H. sapiens* seems to have secondarily evolved a more cebid-like morphology (most

similar to *Saimiri sciureus*) after the split with the *Pan/Homo* last common ancestor, while the bony structure of the saccule in *Pan* is the most flattened with a utricle that is most superiorly displaced, exaggerating the morphology seen in other great apes. While the cause for this disparity is unknown, it is possible that the exaggerated displacement of the utricle and saccule in *Pan* could be the result of enlarged or reorganized ampullar and utricle nerves that pass superficially between these structures, which, rather than having any functional link, would purely be a structural constraint.

Evidence suggests that the human bony vestibule has undergone extensive morphological change away from the general hominid condition. More specifically, a pronounced supraovalic fossa, and reorientation of the bony structure surrounding the utricular macula relative to that of the saccule (Fig. 6a). This reorientation of bony structure in humans may be tied to shifts in head and neck configuration, since endocranial flexion and neck inclination are associated with this type of shape change (Table 3). The orientation of the otolithic organs and their maculae are, indeed, functionally important as differences in maculae orientation alter the orientation of the hair cell bundles. Such differences, in turn, change the directional sensitivity of the otolithic organs[26,45].

Our current ancestral state reconstructions (ASRs) in phylomorphospace suggest that the reorientation of bony structure in humans is convergent with some monkeys (particularly that of *Saimiri sciureus*). This is interesting, as it contrasts with the above functional interpretations of human head posture being linked to otolithic structure. There could be several reasons for this. First, while it is possible that a functional signal is present in the PCA, 3D geometric morphometric methods will also, inherently, pick up non-functional aspects of shape, such as the relative position of the utricle and saccule, and neglect size, which impacts function. Thus, all shape components can reflect a combination of causative factors. Second, the patterns observed here are of bony morphology only. While the bony features landmarked in this study match those of the membranous otolithic organs in humans[35], relationships between bone and membranes could vary in primates, altering functional interpretations when applied to non-human taxa. Lastly, the similarity between *Homo sapiens* and *Saimiri sciureus* could, in part, derive from enlargement of the brain in combination with a restricted size of the petrotympanic region of the cranial base. Indeed, *S. sciureus* exhibits one of highest endocranial volumes relative to cranial base size among platyrrhines[46], and large brains paired with petrotympanic reorganization is well-documented in the *Homo* lineage[47,48].

Nonetheless, our observed connections between otolithic organ orientation and neck inclination may indicate a positional signal in the bony vestibule that can be further explored in two ways: (1) by calibrating ASRs with fossils (particularly those of platyrrhines, hominoids, and early hominins) to better model evolutionary change among clades; and (2) by examining membranous structure of the otolithic organs across primates. Morphological studies on the primate membranous labyrinth (as in refs. 6,35) using micro-CT[49] or synchrotron imaging[50,51] would provide a critical missing element in modeling functional parameters of the otolithic system. This approach would bypass the limitations on functional interpretations in the current study[47,51].

In summary, our research reveals the otolithic system as an important component of the inner ear, distinct from the semicircular canals and the cochlea. This system has undergone significant evolutionary transformations among anthropoids, including humans. Our findings highlight several key morphological shifts in otolithic system evolution among hominoids, marking the divergence of hominids and hylobatids from an ancestral cercopithecid-like form. These evolutionary shifts have culminated in a wide array of vestibule morphologies among hominoids, with humans evolving a distinctive "cebid-like" vestibule structure featuring a notably prominent supraovalic fossa. This exaggerated feature distinguishes our species. These discoveries offer compelling new insights into the evolutionary dynamics of the inner ear, particularly within the human lineage and open up new avenues to reconstruct evolutionary shifts in postural behavior.

Methods

Data acquisition and reconstruction

Our sample includes virtual 3D meshes of 136 right and left inner ears derived from micro-CT (μCT) scans of 14 extant anthropoid species, including a representative sample of modern *H. sapiens* (Supplementary Table 7). Species were chosen following[52] from which data is derived. Existing μCTs were downloaded from MorphoSource (www.morphosource.org) and Morphomuseum (www.morphomuseum.com), with a portion of the sample derived from ref. 53, while other crania were selected from the American Museum of Natural History (AMNH) collections in the Division of Anthropology and scanned using a GE Phoenix Vtome Xs μCT scanner housed within the AMNH Microscopy and Imaging Facility. Isometric voxel size ranged from 33 to 116 μm. Each μCT stack was exported as a series of DCM or TIFF images.

When possible, both left and right ears were included, although this was not possible for some individuals (e.g., single ear meshes downloaded from online repositories). To test for possible bilateral asymmetry in vestibule morphology, we ran a Procrustes analysis of variance (ANOVA) on all ears from our sample, using the "bilat.symmetry" function of the "geomorph" package of R (version 3.5.3[54]). Results indicated no significant bilateral asymmetry present in morphology of the vestibule ($R^2 = 0.0016$; $F = 0.8068$ Z-score = −0.332; $p = 0.635$). Therefore, any potential effects of bilateral asymmetry in the vestibule have no significant impact on our results.

μCT stacks were imported into the visualization software 3D Slicer, version 4.10.1[55]. This allowed axial, sagittal, and coronal plane views of each ear, enabling 3D reconstruction through segmentation. It is possible that errors in fully automated labyrinth segmentation may be introduced at low resolutions that contain image processing artifacts (e.g., partial voluming; for a review, see ref. 44). Therefore, our sample only includes high-resolution μCT stacks that have been checked for any such artifacts. Segmentation of each bony labyrinth was carried out by CMS using a combination of manual and semi-automated thresholding to define best the boundary between the air-filled space of the labyrinth and the surrounding bone. Furthermore, the digital meshes derived from the segmentations were checked for artifacts (e.g., holes in the mesh) using the software Zbrush[56] followed by further refinement of the topology using the "mesh doctor" function in Geomagic Wrap 2017[57].

Statistics and reproducibility

All statistical tests were carried out using the R software package and RStudio integrated development environment[54]. Specific packages and functions used for particular analyses are outlined below. Prior to running statistical models, data on size (i.e., centroid size of the vestibule) was tested for normal distribution using a Shapiro–Wilk normality test. Results indicate significant differences from normality in size (Centroid size: $W = 0.91$, $p = 3.22e{-}07$). Thus, size measures were log-transformed using the natural logarithm (ln) in R when modeling.

Data analyses

Analysis set 1: overall shape variation. To capture the morphology and configuration of the bony casings of the utricle and saccule, a modified set of landmarks (chosen from ref. 35) was placed onto each of our 136 inner ear meshes. For the saccule, a semilandmark patch was placed on the spherical recess using the software Landmark Editor[58] (for further description of landmark placement, see Supplementary Fig. 2 and Supplementary Table 8). This semilandmark patch captures the morphology of the saccular macula and medial portion of the saccule as both adhere to the bony recess itself. For the utricle, only single landmarks were used (landmarks 1–5). These derive from the bony attachment sites of the membrana limitans, which supports the utricle, its macula, and its neural substrate (for further description, see ref. 59). This collection of landmarks has been shown to approximate otolithic system morphology and orientation of the otolithic organ maculae (for a review of the relationship between bony and membranous morphology of the otolithic system, see ref. 35). Landmarking was chosen over surface-based landmark-free methods due to the possibility of artifacts on the meshes altering the

results and adding irrelevant noise to the analysis (for further discussion, see ref. 60).

Intraobserver error and the impact of scan resolution on landmark placement were assessed by repeating landmark placement (ten times) on one *H. sapiens* bony labyrinth (voxel size 89 μm^3) and one *G. gorilla* bony labyrinth (voxel size 116 μm^3). Minimum, maximum, and mean Procrustes distances for the *H. sapiens* error sample were 0.036, 0.084, and 0.056, respectively. Minimum, maximum, and mean Procrustes distances for the *G. gorilla* error sample were 0.049, 0.094, and 0.080, respectively. By comparison, the same values for the total *H. sapiens* and *G. gorilla* samples were 0.052, 0.122, 0.082; and 0.068, 0.153, 0.098, respectively, exceeding those of the error sample and with minimal overlap between the minimum total sample values and maximum error sample values. The intraobserver error, therefore, has a negligible effect on landmark placement.

Landmark coordinates comprising the contour of the semilandmark patch were treated as a sliding semilandmark curve, and thus underwent resampling to arrange coordinates equidistantly from one another using the function "resampleCurve" in the "Morpho" package of R (version 3.5.3[54]). All following statistical analyses were assessed using the "geomorph" package[61] in R. Landmark coordinates underwent generalized Procrustes superimposition (GPA) where coordinates comprising the sliding semilandmark curve were allowed to slide along the tangent directions of their curves, optimizing the homology of landmark positions[62]. Similarly, the nine semilandmark coordinates comprising the remainder of the semilandmark patch were treated as sliding surface semilandmarks during GPA.

Procrustes-aligned landmark coordinates were then subject to a principal component analysis (PCA) to assess overall shape variation among anthropoids. In addition to landmarking, we estimated the angulation between maculae (MA) using a subset of bony landmarks, which have been shown to reflect maculae orientation in humans[35]. This was measured by fitting a plane of best fit to three bony utricle landmarks and three bony saccule landmarks using the software Geomagic Wrap 2017. These include landmarks 1, 3, and 5 for the utricular macula and three landmarks for the saccular macula: the posteriormost, superiormost and anteroinferiormost bounds of the spherical recess (see Supplementary Fig. 2 inset).

Analysis set 2: phylogenetically aligned landmark-based shape analysis. Species represent non-independent cases, and cochlear and SCC morphology, in particular, are known to be significantly influenced by phylogeny among primates[5]. Tests were therefore carried out to determine the level of phylogenetic signal present in bony vestibule size and shape. We used topologies and branch lengths from the GenBank taxonomy consensus tree provided on the 10kTrees website (version 3)[63] (see Supplementary Fig. 3 for the chronophylogenetic tree used in our analyses). Non-independence of data points due to phylogenetic relatedness was tested for by estimating Pagel's lambda (λ)[64], Blomberg's K[65], and K_{mult}[66] using the "phylosig" function from the "phytools" package and "physig" function from the "geomorph" package in R. K_{mult} is a multivariate version of the Bloomberg's K statistic which is able to detect the degree of phylogenetic signal present in a multivariate dataset (i.e., Procrustes shape variables; for a review see ref. 66).

In addition to the standard PCA above, we carried out a phylogenetically aligned components analysis (PaCA) using the "gm.prcomp" function of "geomorph" in R. This was carried out on the mean shape for each species (totaling 14 inner ears). Mean shapes were created using the "mshape" function in "geomorph". The PaCA differs from a PCA in that data are aligned to axes of greatest phylogenetic signal instead of greatest shape variance (for more, information see ref. 67). By doing so, we are able to visualize shape variation most related to phylogeny while minimizing aspects of shape that track with other variables (e.g., body mass, neck inclination).

Analysis set 3: correlations with body mass, endocranial flexion, and head and neck posture. Phylogenetic generalized least-squares (pGLS) models were used to test for relationships between response variables of vestibule size and MA and the explanatory variables of body mass, endocranial flexion, and head and neck orientation (see Supplementary Table 9 for a summary of metrics used). Phylogenetic Procrustes analyses of variance (Phy-ProcD ANOVAs) were used to identify variables that explained significant amounts of variation in bony vestibule shape while taking phylogeny into account. The above tests were carried out using the "pgls" and "procD.pgls" functions of the "caper" and "geomorph" packages in R, respectively. Branch length transformations were estimated for pGLS models using a maximum likelihood approach (and assuming Brownian motion evolution). Lambda cannot be optimized directly in Phy-ProcD ANOVAs. We, therefore, optimized lambda on each shape PC by computing a weighted lambda using the explained shape variance of each PCs as weight. Type I ANOVAs (sequential sum of squares) were used for pGLS models of principal components of shape (from the standard PCA) to determine variables that explain significant variation only after all previous explanatory terms (and phylogeny) have been accounted for. In all pGLS models run with MA as the response variable, the maximum likelihood estimations of lambda were 0. We, therefore, set the pGLS models' lambda value to both the upper bound of its 95% CI and lower bound (0) to account for the highest and lowest likely phylogenetic signal in the model. In cases where there are multiple hypotheses tested, we corrected resulting p values using the Benjamini and Hochberg (also known as fdr) method.

Response variables for the above models include: (1) Centroid size of Procrustes-aligned landmark coordinates (the square root of the sum of squared distances of all the landmarks of an object from their centroid); (2) The ratio of the "bony" utricle centroid size to "bony" saccule centroid size (US ratio); (3) Overall Procrustes shape variables (derived from individual Procrustes coordinates); (4) principal components of Procrustes shape variance that distinguish anthropoid groups and (5) Estimated angulation between maculae (MA). Explanatory variables are as follows: (1) Body mass; (2) Centroid size of Procrustes-aligned landmark coordinates; (3) US ratio; (4) Flexion of the endocranial base (CBA; a measure of endocranial flexion); and (5) Three measures of head and neck orientation. Some of the species included in this study exhibit considerable sexual dimorphism in body size (e.g., *Gorilla gorilla, Pongo pygmaeus, Erythrocebus patas*). Therefore, in these species, only average body mass and inner ear meshes from the majority sex were used. This was done to maximize the number of individuals (and ears) included in each model, rather than running each model independently on smaller samples of males and females (which, in some cases, would only be one ear).

The three measures of head and neck orientation are taken from ref. 52 and include: (1) Neck inclination; (2) Orbit inclination; and (3) Frankfurt inclination (Supplementary Fig. 1). SCC morphology and body mass share a negative allometric relationship[68]. Therefore, under the assumption that the vestibule may follow a similar pattern, the relationship between most response variables and head and neck posture was examined after taking body mass into account (body mass estimates taken from averaged male and female values from refs. 69,70). Measures of CBA were taken from refs. 71,72. CBA is defined here as the angle formed from the intersection of the planum sphenoideum (measured from most anterosuperior midline point on the sloping surface in which cribriform plate is set to clival point) and the clival plane (measured as endobasion to clival point) (Supplementary Fig. 4). This measure captures endocranial base flexion and was chosen to maintain consistency with[52] as CBA is incorporated into their analyses of primate head and neck orientation.

Reporting summary

Further information on research design is available in the Nature Portfolio Reporting Summary linked to this article.

Data availability

All segmentations of non-human primate bony labyrinths generated during this study are available at https://www.morphosource.org/projects/000642639. Human segmentations can only be shared with permission of curating institution. Other data generated and analyzed for this study are available from the corresponding author upon reasonable request.

Received: 15 August 2024; Accepted: 25 September 2024;
Published online: 02 October 2024

References

1. Goldberg, J. M. et al. The vestibular system in everyday life. In *The Vestibular System: A Sixth Sense* (ed. Goldberg, J. M.) 1–18 (Oxford University Press, 2012).
2. Bast, T. H. & Anson, B. J. *The Temporal Bone and the Ear* (C.C. Thomas, 1949).
3. Urciuoli, A. et al. The evolution of the vestibular apparatus in apes and humans. *Elife* **9**, 1–33 (2020).
4. Spoor, F. & Zonneveld, F. Comparative review of the human bony labyrinth. *Yearb. Phys. Anthropol.* **41**, 211–251 (1998).
5. Morimoto, N. et al. Variation of bony labyrinthine morphology in Mio–Plio–Pleistocene and modern anthropoids. *Am. J. Phys. Anthropol.* **173**, 276–292 (2020).
6. David, R., Stoessel, A., Berthoz, A., Spoor, F. & Bennequin, D. Assessing morphology and function of the semicircular duct system: introducing new in-situ visualization and software toolbox. *Sci. Rep.* **6**, 32772 (2016).
7. Hunt, K. D. et al. Standardized descriptions of primate locomotor and postural modes. *Primates* **37**, 363–387 (1996).
8. Williams, S. A., Prang, T. C., Russo, G. A., Young, N. M. & Gebo, D. L. African apes and the evolutionary history of orthogrady and bipedalism. *Yearbook Biol. Anthropol.* **181**, 58–80 (2023).
9. Yang, A. & Hullar, T. E. Relationship of semicircular canal size to vestibular-nerve afferent sensitivity in mammals. *J. Neurophysiol.* **98**, 3197–3205 (2007).
10. Rabbitt, R. D. Semicircular canal biomechanics in health and disease. *J. Neurophysiol.* **121**, 732–755 (2019).
11. Rabbitt, R. D., Damiano, E. R. & Grant, J. W. Biomechanics of the semicircular canals and otolith organs. in *The Vestibular System* (eds Highstein, S. M., Fay, R. R. & Popper, A. N.) 153–201 (Springer, 2004).
12. Steinhausen, W. Über die Beobachtung der Cupula in den Bogengangsampullen des Labyrinths des lebenden Hechts. *Pflug. Arch. Gesamt. Physiol. Menschen Tiere* **232**, 500–512 (1933).
13. van Egmond, A. A. J., Groen, J. J. & Jongkees, L. B. W. The mechanics of the semicircular canal. *J. Physiol.* **110**, 1–17 (1949).
14. Fitzpatrick, R. C., Butler, J. E. & Day, B. L. Resolving head rotation for human bipedalism. *Curr. Biol.* **16**, 1509–1514 (2006).
15. Walker, A., Ryan, T. M., Silcox, M. T., Simons, E. L. & Spoor, F. The semicircular canal system and locomotion: the case of extinct lemuroids and lorisoids. *Evol. Anthropol.* **17**, 135–145 (2008).
16. Silcox, M. T. et al. Semicircular canal system in early primates. *J. Hum. Evol.* **56**, 315–327 (2009).
17. Ryan, T. M. et al. Evolution of locomotion in anthropoidea: the semicircular canal evidence. *Proc. R. Soc. B Biol. Sci.* **279**, 3467–3475 (2012).
18. Spoor, F. et al. The primate semicircular canal system and locomotion. *Proc. Natl. Acad. Sci. USA* **104**, 10808–10812 (2007).
19. Spoor, F., Wood, B. & Zonneveld, F. Implications of early hominid labyrinthine morphology for evolution of human bipedal locomotion. *Nature* **369**, 645–648 (1994).
20. Spoor, F., Wood, B. & Zonneveld, F. Evidence for a link between human semicircular canal size and bipedal behaviour. *J. Hum. Evol.* **30**, 183–187 (1996).
21. Schellhorn, R. A potential link between lateral semicircular canal orientation, head posture, and dietary habits in extant rhinos (Perissodactyla, Rhinocerotidae). *J. Morphol.* **279**, 50–61 (2018).
22. Coutier, F., Hautier, L., Cornette, R., Amson, E. & Billet, G. Orientation of the lateral semicircular canal in Xenarthra and its links with head posture and phylogeny. *J. Morphol.* **278**, 704–717 (2017).
23. Spoor, F., Hublin, J. J., Braun, M. & Zonneveld, F. The bony labyrinth of Neanderthals. *J. Hum. Evol.* **44**, 141–165 (2003).
24. le Maître, A., Schuetz, P., Vignaud, P. & Brunet, M. New data about semicircular canal morphology and locomotion in modern hominoids. *J. Anat.* **231**, 95–109 (2017).
25. Rosenhall, U. Vestibular macular mapping in man. *Ann. Otol.* **81**, 339–351 (1972).
26. Tribukait, A. & Rosenhall, U. Directional sensitivity of the human macula utriculi based on morphological characteristics. *Audio. Neurootol.* **6**, 98–107 (2001).
27. Igarashi, M., O-Uchi, T., Isago, H. & Wright, W. K. Utricular and saccular volumetry in human temporal bones. *Acta Otolaryngol.* **95**, 75–80 (1983).
28. Takagi, A. & Sando, I. Computer-aided three-dimensional reconstruction and measurement of the vestibular end-organs. *Otolaryngol. Head. Neck Surg.* **98**, 195–202 (1988).
29. Backous, D. D., Aboujaoude, E. S., Minor, L. B. & Nager, G. T. Relationship of the utriculus and sacculus to the stapes footplate: anatomic. *Ann. Orol. Rhinol. Laryngol.* **548**, 553 (1999).
30. Dimiccoli, M. et al. Striola magica: A functional explanation of otolith geometry. *J. Comput. Neurosci.* **35**, 125–154 (2013)
31. Mukherjee, P. et al. Three-dimensional analysis of the vestibular end organs in relation to the stapes footplate and piston placement. *Otol. Neurotol.* **32**, 367–372 (2011).
32. Day, B. L. & Fitzpatrick, R. C. The vestibular system. *J. Appl. Physiol.* **15**, R583–R586 (2004).
33. Cathers, I., Day, B. L. & Fitzpatrick, R. C. Otolith and canal reflexes in human standing. *J. Physiol.* **563**, 229–234 (2005).
34. Jaeger, R., Takagi, A. & Haslwanter, T. Modeling the relation between head orientations and otolith responses in humans. *Hear. Res.* **173**, 29–42 (2002).
35. Smith, C. M., Curthoys, I. S. & Laitman, J. T. First evidence of the link between internal and external structure of the human inner ear otolith system using 3D morphometric modeling. *Sci. Rep.* **13**, 4840 (2023).
36. Hunt, K. D. Positional behavior in the Hominoidea. *Int. J. Primatol.* **12**, 95–118 (1991).
37. Almécija, S. et al. Fossil apes and human evolution. *Science* **372**, eabb4363 (2021).
38. Hunt, K. D. Why are there apes? Evidence for the co-evolution of ape and monkey ecomorphology. *J. Anat.* **228**, 630–685 (2016).
39. Young, E. D., Fernández, C. & Goldberg, J. M. Responses of squirrel monkey vestibular neurons to audio-frequency sound and head vibration. *Acta Otolaryngol.* **84**, 352–360 (1977).
40. Geissmann, T. Duet songs of the siamang, Hylobates syndactylus: I. Structure and organisation. *Primate Rep.* **56**, 33–60 (2000).
41. Todd, N. P. M. & Merker, B. Siamang gibbons exceed the saccular threshold: intensity of the song of Hylobates syndactylus. *J. Acoust. Soc. Am.* **115**, 3077–3080 (2004).
42. Pugh, K. D. et al. The reconstructed cranium of *Pierolapithecus* and the evolution of the great ape face. *Proc. Natl. Acad. Sci. USA* **120**, e2218778120 (2023).
43. Grabowski, M. & Jungers, W. L. Evidence of a chimpanzee-sized ancestor of humans but a gibbon-sized ancestor of apes. *Nat. Commun.* https://doi.org/10.1038/s41467-017-00997-4 (2017).
44. Curthoys, I. S., Uzun-Coruhlu, H., Wong, C. C., Jones, A. S. & Bradshaw, A. P. The configuration and attachment of the utricular and saccular maculae to the temporal bone. *Ann. N. Y. Acad. Sci.* **1164**, 13–18 (2009).
45. Tribukait, A., Rosenhall, U. & Österdahl, B. Morphological characteristics of the human macula sacculi. *Audiol. Neurotol.* **10**, 90–96 (2005).
46. Aristide, L. et al. Brain shape convergence in the adaptive radiation of New World monkeys. *Proc. Natl. Acad. Sci. USA* **113**, 2158–2163 (2016).
47. Lieberman, D. E., Ross, C. F. & Ravosa, M. J. The primate cranial base: ontogeny, function, and integration. *Am. J. Phys. Anthropol.* **31**, 117–169 (2000).

48. Nevell, L. & Wood, B. Cranial base evolution within the hominin clade. *J. Anat.* **212**, 455–468 (2008).
49. Uzun, H., Curthoys, I. S. & Jones, A. S. A new approach to visualizing the membranous structures of the inner ear—high resolution X-ray micro-tomography. *Acta Otolaryngol.* **127**, 568–573 (2007).
50. Elfarnawany, M. et al. Micro-CT versus synchrotron radiation phase contrast imaging of human cochlea. *J. Microsc.* **265**, 349–357 (2017).
51. Li, H. et al. A synchrotron and micro-CT study of the human endolymphatic duct system: is Meniere's disease caused by an acute endolymph backflow? *Front. Surg.* **8**, 662530 (2021).
52. Strait, D. S. & Ross, C. F. Kinematic data on primate head and neck posture: implications for the evolution of basicranial flexion and an evaluation of registration planes used in paleoanthropology. *Am. J. Phys. Anthropol.* **108**, 205–222 (1999).
53. Beaudet, A. et al. Upper third molar internal structural organization and semicircular canal morphology in Plio-Pleistocene South African cercopithecoids. *J. Hum. Evol.* **95**, 104–120 (2016).
54. R Core Team. *R: A Language and Environment for Statistical Computing* (R Foundation for Statistical Computing, 2020).
55. Fedorov, A. et al. 3D Slicer as an image computing platform for the quantitative imaging network. *Magn. Reson. Imaging* **30**, 1323–1341 (2012).
56. Maxon Computer GmbH, Zbrush [Software]. Retrieved from https://www.maxon.net (2023).
57. 3DSystems, Geomagic [Software]. Retrieved from https://www.3dsystems.com (2017).
58. Wiley, D. F. et al. Evolutionary morphing. *Proc. IEEE Vis.* 431–438 (2005).
59. Smith, C. M., Curthoys, I. S., Mukherjee, P., Wong, C. & Laitman, J. T. Three-dimensional visualization of the human membranous labyrinth: the membrana limitans and its role in vestibular form. *Anat. Rec.* **305**, 1037–1050 (2022).
60. Pomidor, B. J., Makedonska, J. & Slice, D. E. A landmark-free method for three-dimensional shape analysis. *PLoS ONE* **11**, 1–18 (2016).
61. Baken, E. K., Collyer, M. L., Kaliontzopoulou, A. & Adams, D. C. geomorph v4.0 and gmShiny: enhanced analytics and a new graphical interface for a comprehensive morphometric experience. *Methods Ecol. Evol.* **12**, 2355–2363 (2021).
62. Gunz, P. & Mitteroecker, P. Semilandmarks: a method for quantifying curves and surfaces. *Hystrix* **24**, 103–109 (2013).
63. Arnold, C., Matthews, L. J. & Nunn, C. L. The 10kTrees website: a new online resource for primate phylogeny. *Evol. Anthropol.* **19**, 114–118 (2010).
64. Pagel, M. Inferring the historical patterns of biological evolution. *Nature* **401**, 877–884 (1999).
65. Blomberg, S. P., Garland, T. & Ives, A. R. Testing for phylogenetic signal in comparative data: behavioral traits are more labile. *Evolution* **57**, 717–745 (2003).
66. Adams, D. C. A generalized K statistic for estimating phylogenetic signal from shape and other high-dimensional multivariate data. *Syst. Biol.* **63**, 685–697 (2014).
67. Collyer, M. L. & Adams, D. C. Phylogenetically aligned component analysis. *Methods Ecol. Evol.* **12**, 359–372 (2021).
68. Jones, G. & Spells, K. A theoretical and comparative study of the functional dependence of the semicircular canal upon its physical dimensions. *Proc. R. Soc. Lond. B* **157**, 403–419 (1963).
69. Smith, R. J. & Jungers, W. L. Body mass in comparative primatology. *J. Hum. Evol.* **32**, 523–559 (1997).
70. Fleagle, J. *Primate Adaptation and Evolution* (Academic Press, 2013).
71. Ross, C. F. & Ravosa, M. J. Basicranial flexion, relative brain size, and facial kyphosis in nonhuman primates. *Am. J. Phys. Anthropol.* **91**, 305–324 (1993).
72. Ross, C. F. Basicranial flexion, relative brain size, and facial kyphosis in homo sapiens and some fossil hominids. *Am. J. Phys. Anthropol.* **98**, 575–593 (1995).

Acknowledgements

This research was supported by an NSF Doctoral Dissertation Research Improvement Grant (award #: 2051335), the Calleva Foundation, the R + D + I project PID2020-116908GB-I00 (MCIN/AEI/10.13039/501100011033/), and the Generalitat de Catalunya (CERCA Programme). The authors thank Amélie Beaudet and colleagues for providing 3D surface models of the inner ear that comprise a portion of our cercopithecid sample, as well as MorphoSource and MorphoMuseuM and the following original sources of digital content from which a portion of the current sample derives: the Museum of Comparative Zoology, Harvard University; the American Museum of Natural History, Department of Mammalogy; and the National Museum of Natural History, Department of Vertebrate Zoology. The authors would also like to thank Eric Delson, Will Harcourt-Smith, Tim Smith, and David Friedland for generously providing helpful feedback on this manuscript.

Author contributions

Conceptualization: C.M.S. (lead), R.D., A.S.H., S.A., and J.T.L. Methodology: C.M.S., R.D., A.S.H., and S.A. Formal analyses: C.M.S. and R.D. Data curation: C.M.S. and R.D. Writing: C.M.S. (lead), R.D., A.S.H., S.A., and J.T.L. Supervision: A.S.H., S.A., and J.T.L. Funding acquisition: C.M.S., R.D., A.S.H., S.A., and J.T.L.

Competing interests

The authors declare no competing interests.

Additional information

Supplementary information The online version contains supplementary material available at https://doi.org/10.1038/s42003-024-06966-0.

Correspondence and requests for materials should be addressed to Christopher M. Smith.

Peer review information *Communications Biology* thanks Mary Silcox and the other, anonymous, reviewer(s) for their contribution to the peer review of this work. Primary Handling Editor: Jasmine Pan. A peer review file is available.